Electronic Supplementary Material (ESI) for Journal of Materials Chemistry C.
This journal is © The Royal Society of Chemistry 2021

Electronic Supplementary Information (ESI)
for

Impact of noncovalent interactions on structural and photophysical properties of zero-dimensional tellurium(IV) perovskites

Aaron D. Nicholas,[1] Benjamin W. Walusiak,[1] Leah C. Garman,[1] Mehrun N. Huda,[1] Christopher L. Cahill[1]
[1]Department of Chemistry, The George Washington University, 800 22nd Street, NW, Washington, D.C. 20052, United States

Email: cahill@gwu.edu

Electronic Supplementary Information Section

Figure S1. ORTEP drawing of compound **1**, $(C_5H_6N)_2[TeCl_6]$.

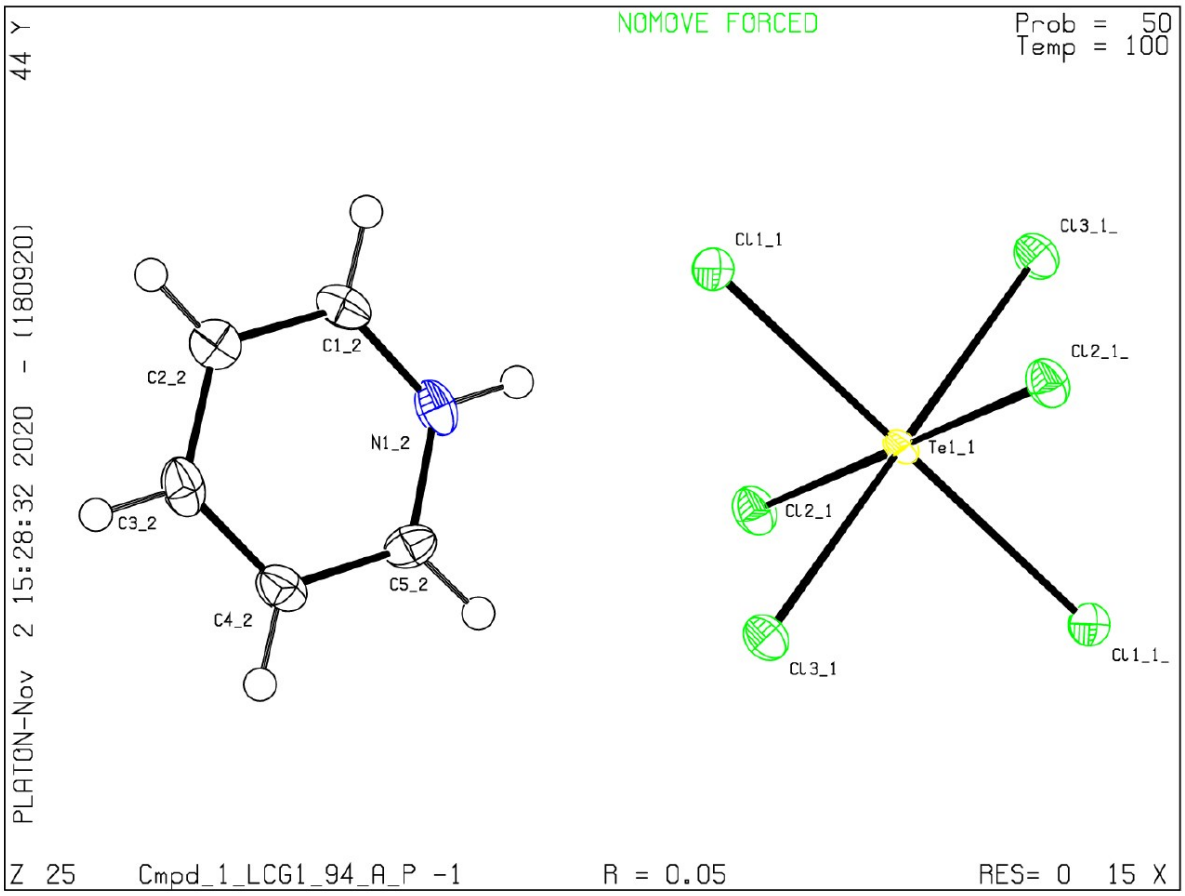

Table S1. Bond distances and angles for compound **1**, $(C_5H_5NCl)_2[TeCl_6]$.

Atom1	Atom2	Atom3	Angle	Atom1	Atom2	Length
H6_2	N1_2	C5_2	118.1	N1_2	H6_2	0.86
H6_2	N1_2	C1_2	118.2	N1_2	C5_2	1.331(7)
C5_2	N1_2	C1_2	123.7(5)	N1_2	C1_2	1.327(6)
H2_2	C2_2	C3_2	120.7	C2_2	H2_2	0.93
H2_2	C2_2	C1_2	120.6	C2_2	C3_2	1.382(8)
C3_2	C2_2	C1_2	118.7(5)	C2_2	C1_2	1.368(7)
C2_2	C3_2	H3_2	120.1	C3_2	H3_2	0.93
C2_2	C3_2	C4_2	119.7(5)	C3_2	C4_2	1.381(7)
H3_2	C3_2	C4_2	120.2	C4_2	H4_2	0.93
C3_2	C4_2	H4_2	120.1	C4_2	C5_2	1.366(7)
C3_2	C4_2	C5_2	119.7(5)	C5_2	H5_2	0.93
H4_2	C4_2	C5_2	120.2	C1_2	H1_2	0.93
N1_2	C5_2	C4_2	118.6(5)	Te1_1	Cl2_1	2.565
N1_2	C5_2	H5_2	120.7	Te1_1	Cl3_1	2.528
C4_2	C5_2	H5_2	120.7	Te1_1	Cl1_1	2.521
N1_2	C1_2	C2_2	119.6(5)	Te1_1	Cl2_1	2.565
N1_2	C1_2	H1_2	120.2	Te1_1	Cl3_1	2.528
C2_2	C1_2	H1_2	120.2	Te1_1	Cl1_1	2.521
Cl2_1	Te1_1	Cl3_1	87.9			
Cl2_1	Te1_1	Cl1_1	89.2			
Cl2_1	Te1_1	Cl2_1	180.0			
Cl2_1	Te1_1	Cl3_1	92.1			
Cl2_1	Te1_1	Cl1_1	90.8			
Cl3_1	Te1_1	Cl1_1	89.3			
Cl3_1	Te1_1	Cl2_1	92.1			
Cl3_1	Te1_1	Cl3_1	180.0			
Cl3_1	Te1_1	Cl1_1	90.7			
Cl1_1	Te1_1	Cl2_1	90.8			
Cl1_1	Te1_1	Cl3_1	90.7			
Cl1_1	Te1_1	Cl1_1	180.0			
Cl2_1	Te1_1	Cl3_1	87.9			
Cl2_1	Te1_1	Cl1_1	89.2			
Cl3_1	Te1_1	Cl1_1	89.3			

Figure S2. ORTEP drawing of compound **2**, $(C_5H_5NCl)_2[TeCl_6]$.

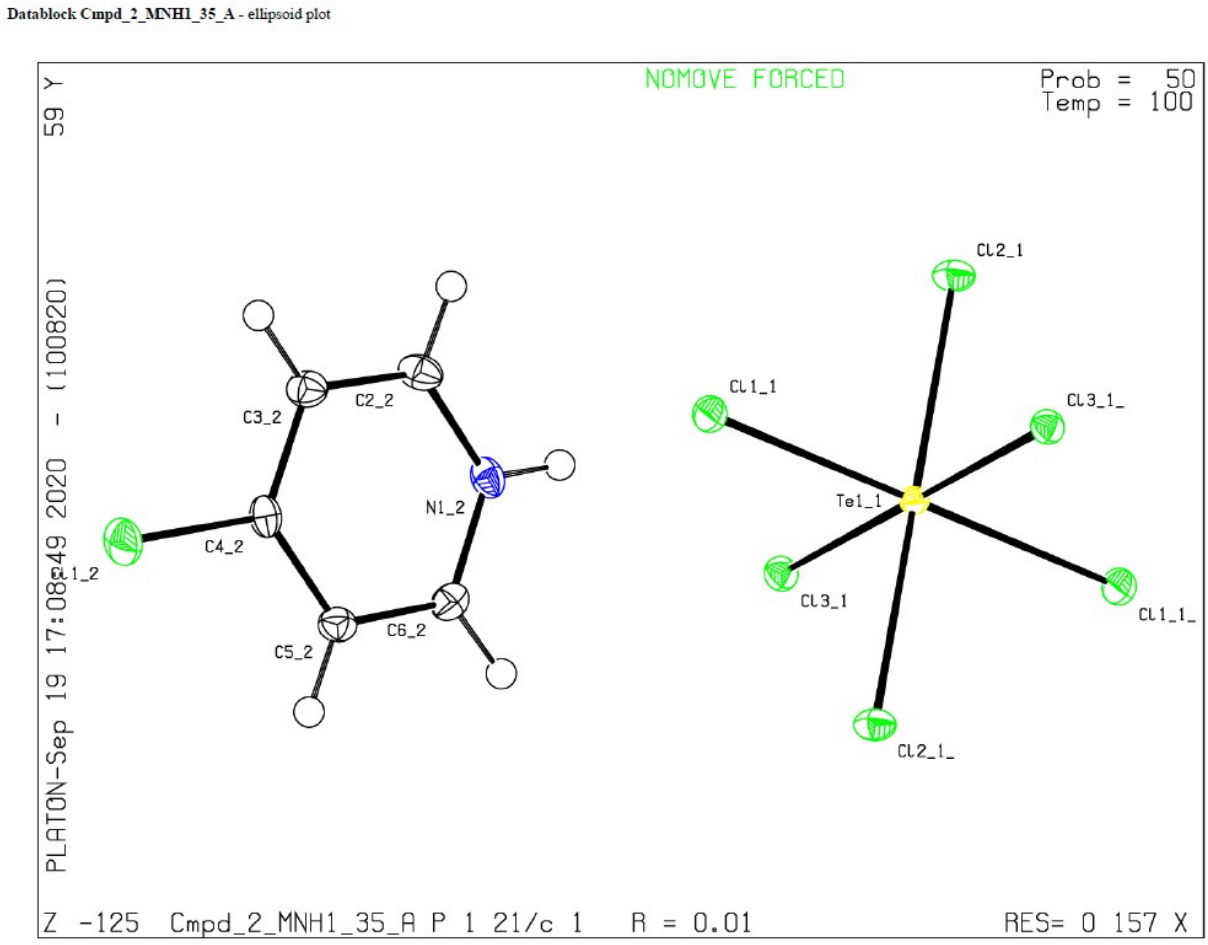

Table S2. Bond distances and angles for compound **2**, $(C_5H_5NCl)_2[TeCl_6]$.

Atom1	Atom2	Atom3	Angle	Atom1	Atom2	Length
Cl2_1	Te1_1	Cl3_1	91.4	Te1_1	Cl2_1	2.531
Cl2_1	Te1_1	Cl1_1	90.0	Te1_1	Cl3_1	2.5609
Cl2_1	Te1_1	Cl2_1	180.0	Te1_1	Cl1_1	2.5281
Cl2_1	Te1_1	Cl3_1	88.6	Te1_1	Cl2_1	2.531
Cl2_1	Te1_1	Cl1_1	90.0	Te1_1	Cl3_1	2.5609
Cl3_1	Te1_1	Cl1_1	91.5	Te1_1	Cl1_1	2.5281
Cl3_1	Te1_1	Cl2_1	88.6	N1_2	H1_2	0.88
Cl3_1	Te1_1	Cl3_1	180.0	N1_2	C2_2	1.340(2)
Cl3_1	Te1_1	Cl1_1	88.5	N1_2	C6_2	1.342(2)
Cl1_1	Te1_1	Cl2_1	90.0	Cl1_2	C4_2	1.717(1)
Cl1_1	Te1_1	Cl3_1	88.5	C2_2	H2_2	0.95
Cl1_1	Te1_1	Cl1_1	180.0	C2_2	C3_2	1.375(2)
Cl2_1	Te1_1	Cl3_1	91.4	C3_2	H3_2	0.95
Cl2_1	Te1_1	Cl1_1	90.0	C3_2	C4_2	1.387(2)
Cl3_1	Te1_1	Cl1_1	91.5	C4_2	C5_2	1.394(2)
H1_2	N1_2	C2_2	118.5	C5_2	H5_2	0.95
H1_2	N1_2	C6_2	118.5	C5_2	C6_2	1.373(2)
C2_2	N1_2	C6_2	122.9(1)	C6_2	H6_2	0.95
N1_2	C2_2	H2_2	120.0			
N1_2	C2_2	C3_2	120.0(1)			
H2_2	C2_2	C3_2	120.0			
C2_2	C3_2	H3_2	121.0			
C2_2	C3_2	C4_2	118.1(1)			
H3_2	C3_2	C4_2	120.9			
Cl1_2	C4_2	C3_2	119.7(1)			
Cl1_2	C4_2	C5_2	119.4(1)			
C3_2	C4_2	C5_2	121.0(1)			
C4_2	C5_2	H5_2	120.9			
C4_2	C5_2	C6_2	118.2(1)			
H5_2	C5_2	C6_2	120.9			
N1_2	C6_2	C5_2	119.8(1)			
N1_2	C6_2	H6_2	120.1			
C5_2	C6_2	H6_2	120.1			

Figure S3. ORTEP drawing of compound **3**, $(C_5H_5NBr)_2[TeCl_6]$.

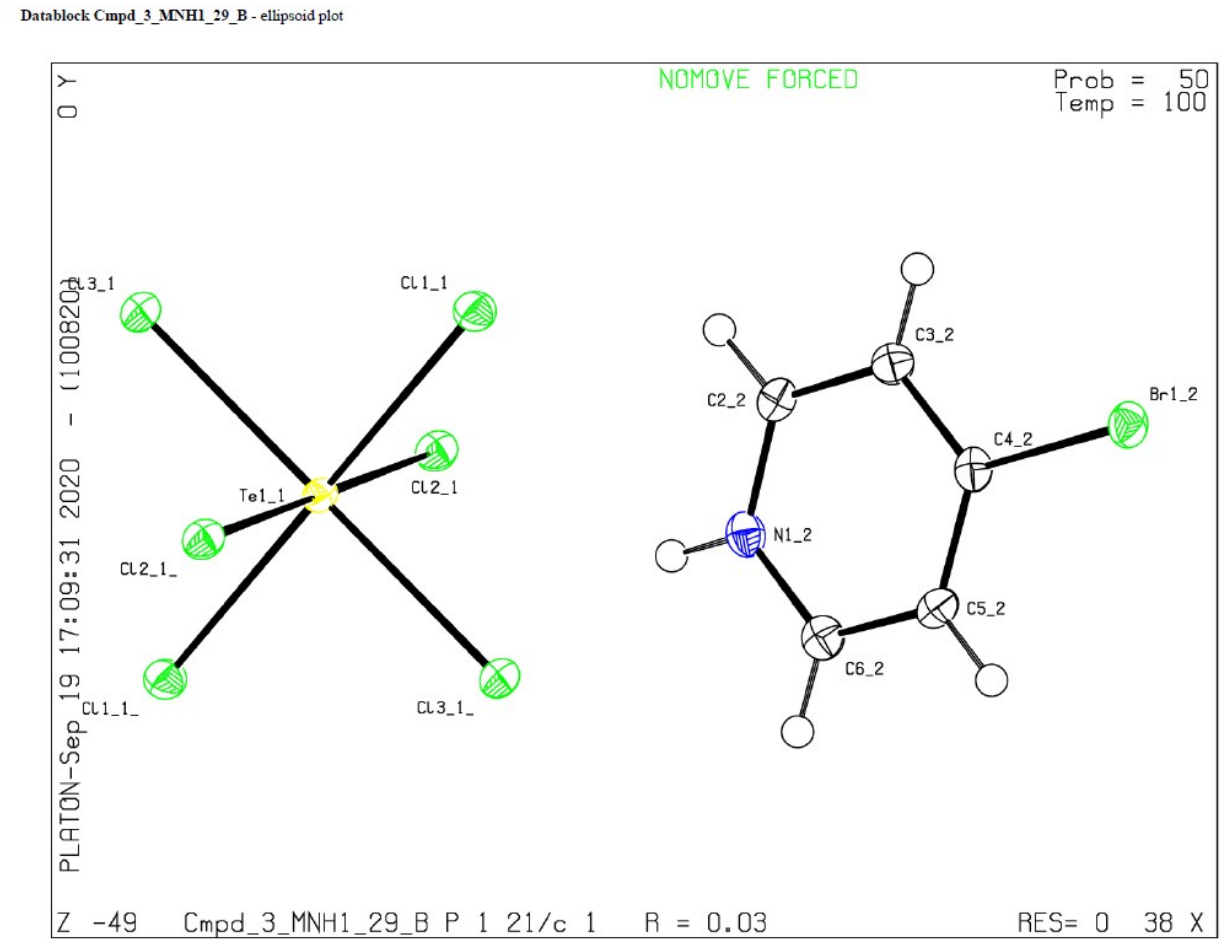

Table S3. Bond distances and angles for compound **3**, $(C_5H_5NBr)_2[TeCl_6]$.

Atom1	Atom2	Atom3	Angle	Atom1	Atom2	Length
Cl2_1	Te1_1	Cl3_1	89.3	Te1_1	Cl2_1	2.5581
Cl2_1	Te1_1	Cl1_1	89.0	Te1_1	Cl3_1	2.5302
Cl2_1	Te1_1	Cl2_1	180.0	Te1_1	Cl1_1	2.5305
Cl2_1	Te1_1	Cl3_1	90.7	Te1_1	Cl2_1	2.5581
Cl2_1	Te1_1	Cl1_1	91.0	Te1_1	Cl3_1	2.5302
Cl3_1	Te1_1	Cl1_1	90.3	Te1_1	Cl1_1	2.5305
Cl3_1	Te1_1	Cl2_1	90.7	N1_2	H1_2	0.88
Cl3_1	Te1_1	Cl3_1	180.0	N1_2	C2_2	1.342(4)
Cl3_1	Te1_1	Cl1_1	89.7	N1_2	C6_2	1.340(4)
Cl1_1	Te1_1	Cl2_1	91.0	Br1_2	C4_2	1.871(3)
Cl1_1	Te1_1	Cl3_1	89.7	C2_2	H2_2	0.949
Cl1_1	Te1_1	Cl1_1	180.0	C2_2	C3_2	1.374(5)
Cl2_1	Te1_1	Cl3_1	89.3	C3_2	H3_2	0.95
Cl2_1	Te1_1	Cl1_1	89.0	C3_2	C4_2	1.396(5)
Cl3_1	Te1_1	Cl1_1	90.3	C4_2	C5_2	1.389(4)
H1_2	N1_2	C2_2	118.5	C5_2	H5_2	0.95
H1_2	N1_2	C6_2	118.6	C5_2	C6_2	1.369(5)
C2_2	N1_2	C6_2	122.9(3)	C6_2	H6_2	0.95
N1_2	C2_2	H2_2	120.3			
N1_2	C2_2	C3_2	119.5(3)			
H2_2	C2_2	C3_2	120.2			
C2_2	C3_2	H3_2	120.7			
C2_2	C3_2	C4_2	118.5(3)			
H3_2	C3_2	C4_2	120.8			
Br1_2	C4_2	C3_2	119.9(2)			
Br1_2	C4_2	C5_2	119.6(2)			
C3_2	C4_2	C5_2	120.5(3)			
C4_2	C5_2	H5_2	120.8			
C4_2	C5_2	C6_2	118.4(3)			
H5_2	C5_2	C6_2	120.8			
N1_2	C6_2	C5_2	120.1(3)			
N1_2	C6_2	H6_2	120.0			
C5_2	C6_2	H6_2	119.9			

Figure S4. ORTEP drawing for compound **4**, $(C_5H_5NI)_2[TeCl_6]$.

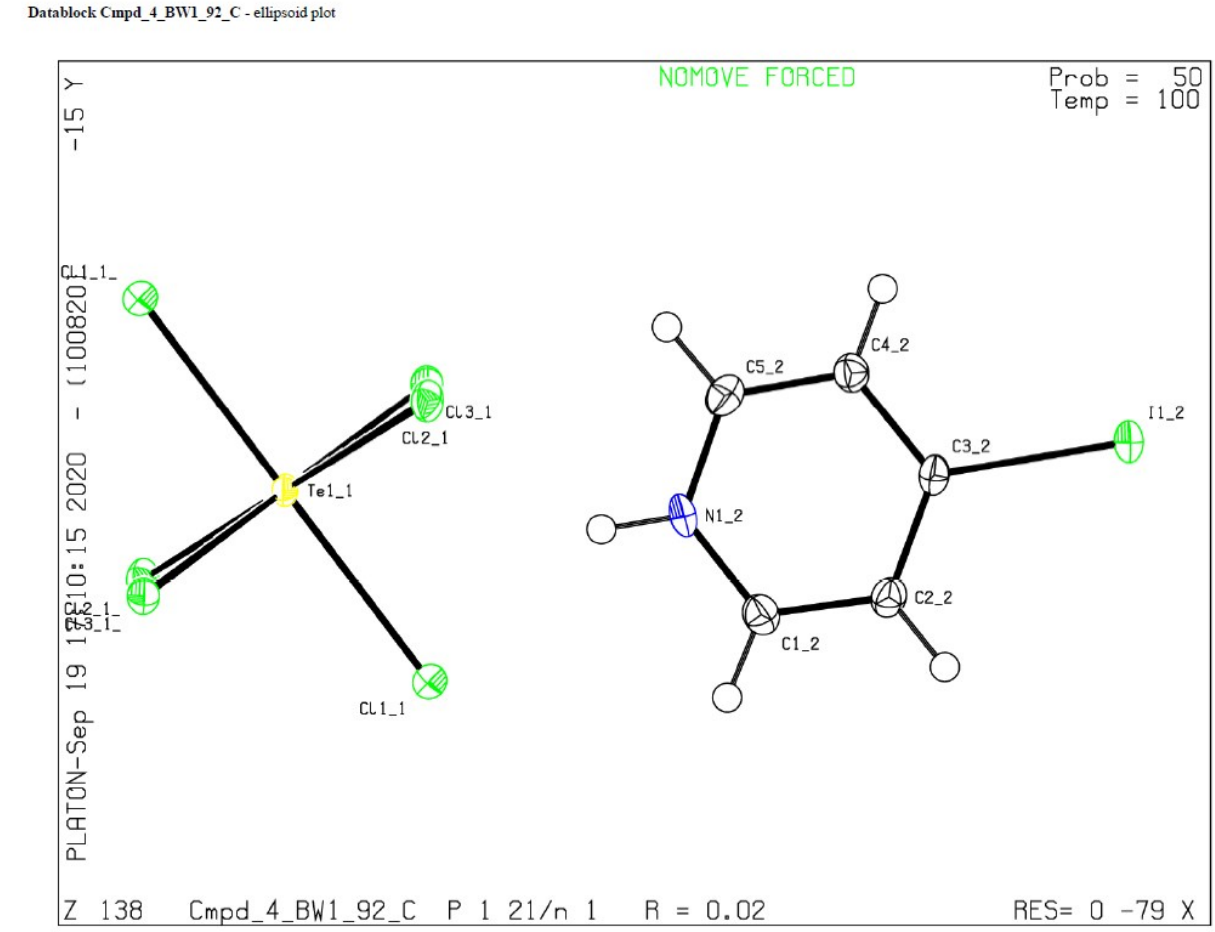

Table S4. Bond distances and angles for compound **4**, $(C_5H_5NBr)_4InBr_{4.36}Cl_{5.64}$.

Atom1	Atom2	Atom3	Angle	Atom1	Atom2	Length
Cl2_1	Te1_1	Cl3_1	88.5	Te1_1	Cl2_1	2.5463
Cl2_1	Te1_1	Cl1_1	88.9	Te1_1	Cl3_1	2.5583
Cl2_1	Te1_1	Cl2_1	180.0	Te1_1	Cl1_1	2.5514
Cl2_1	Te1_1	Cl3_1	91.6	Te1_1	Cl2_1	2.5463
Cl2_1	Te1_1	Cl1_1	91.1	Te1_1	Cl3_1	2.5583
Cl3_1	Te1_1	Cl1_1	87.6	Te1_1	Cl1_1	2.5514
Cl3_1	Te1_1	Cl2_1	91.6	N1_2	H6_2	0.88
Cl3_1	Te1_1	Cl3_1	180.0	N1_2	C5_2	1.349(5)
Cl3_1	Te1_1	Cl1_1	92.4	N1_2	C1_2	1.341(4)
Cl1_1	Te1_1	Cl2_1	91.1	I1_2	C3_2	2.095(3)
Cl1_1	Te1_1	Cl3_1	92.4	C2_2	H2_2	0.95
Cl1_1	Te1_1	Cl1_1	180.0	C2_2	C3_2	1.387(5)
Cl2_1	Te1_1	Cl3_1	88.5	C2_2	C1_2	1.369(4)
Cl2_1	Te1_1	Cl1_1	88.9	C3_2	C4_2	1.394(4)
Cl3_1	Te1_1	Cl1_1	87.6	C4_2	H4_2	0.95
H6_2	N1_2	C5_2	118.7	C4_2	C5_2	1.364(4)
H6_2	N1_2	C1_2	118.7	C5_2	H5_2	0.95
C5_2	N1_2	C1_2	122.6(3)	C1_2	H1_2	0.95
H2_2	C2_2	C3_2	121.1			
H2_2	C2_2	C1_2	121.0			
C3_2	C2_2	C1_2	117.9(3)			
I1_2	C3_2	C2_2	119.9(2)			
I1_2	C3_2	C4_2	119.3(2)			
C2_2	C3_2	C4_2	120.8(3)			
C3_2	C4_2	H4_2	120.6			
C3_2	C4_2	C5_2	118.9(3)			
H4_2	C4_2	C5_2	120.5			
N1_2	C5_2	C4_2	119.3(3)			
N1_2	C5_2	H5_2	120.3			
C4_2	C5_2	H5_2	120.3			
N1_2	C1_2	C2_2	120.4(3)			
N1_2	C1_2	H1_2	119.7			
C2_2	C1_2	H1_2	119.8			

Figure S5. ORTEP drawing of compound **5**, $(C_5H_6N)_2$ [$TeBr_6$].

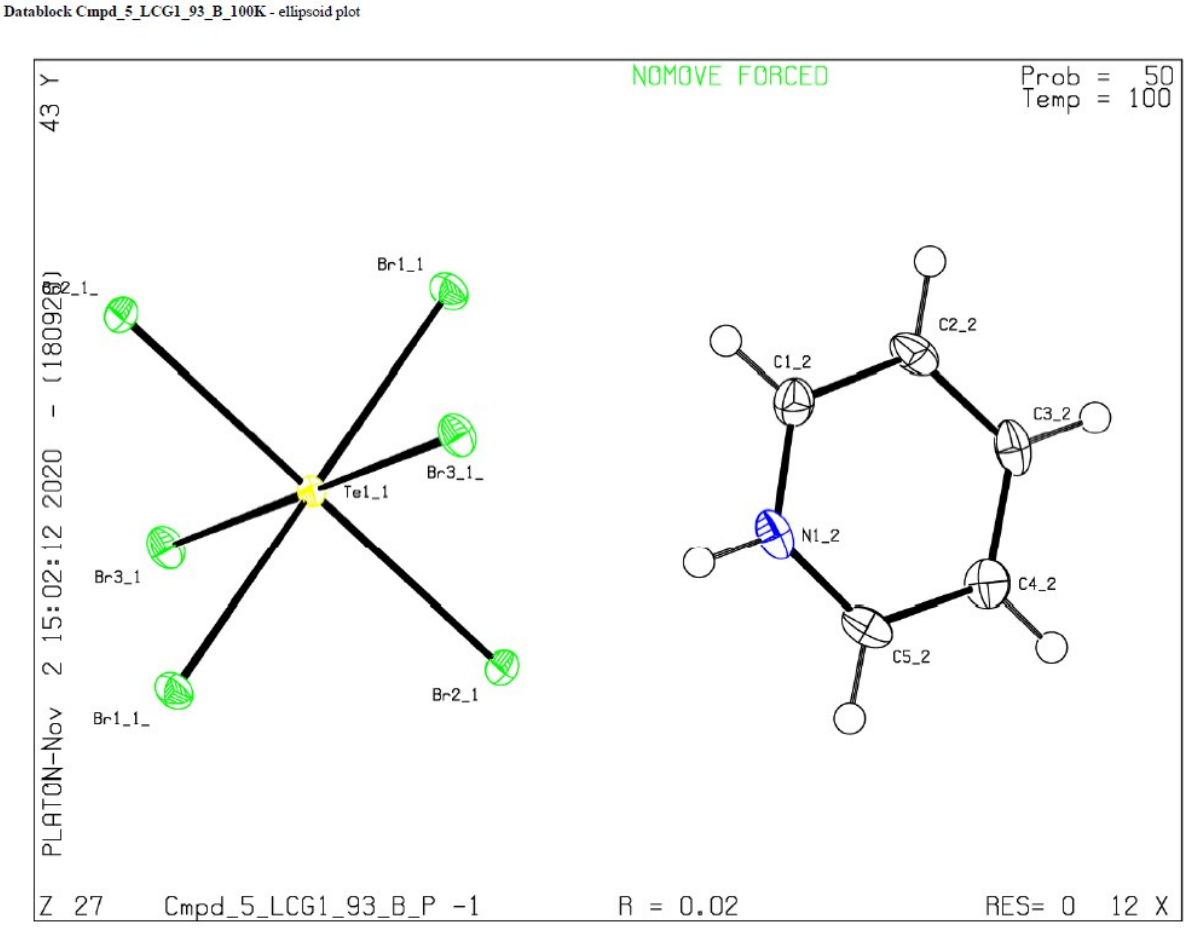

Table S5. Bond distances and angles for compound **5**, $(C_5H_6N)_2$ $[TeBr_6]$.

Atom1	Atom2	Atom3	Angle	Atom1	Atom2	Length
Br1_1	Te1_1	Br2_1	89.4	Br1_1	Te1_1	2.689
Br1_1	Te1_1	Br3_1	92.6	Te1_1	Br2_1	2.68
Br1_1	Te1_1	Br1_1	180.0	Te1_1	Br3_1	2.719
Br1_1	Te1_1	Br2_1	90.6	Te1_1	Br1_1	2.689
Br1_1	Te1_1	Br3_1	87.4	Te1_1	Br2_1	2.68
Br2_1	Te1_1	Br3_1	90.3	Te1_1	Br3_1	2.719
Br2_1	Te1_1	Br1_1	90.6	C1_2	H1_2	0.93
Br2_1	Te1_1	Br2_1	180.0	C1_2	N1_2	1.335(4)
Br2_1	Te1_1	Br3_1	89.8	C1_2	C2_2	1.370(5)
Br3_1	Te1_1	Br1_1	87.4	N1_2	H6_2	0.86
Br3_1	Te1_1	Br2_1	89.8	N1_2	C5_2	1.337(4)
Br3_1	Te1_1	Br3_1	180.0	C2_2	H2_2	0.93
Br1_1	Te1_1	Br2_1	89.4	C2_2	C3_2	1.395(4)
Br1_1	Te1_1	Br3_1	92.6	C3_2	H3_2	0.93
Br2_1	Te1_1	Br3_1	90.3	C3_2	C4_2	1.384(5)
H1_2	C1_2	N1_2	120.2	C4_2	H4_2	0.93
H1_2	C1_2	C2_2	120.2	C4_2	C5_2	1.369(4)
N1_2	C1_2	C2_2	119.6(3)	C5_2	H5_2	0.93
C1_2	N1_2	H6_2	118.4			
C1_2	N1_2	C5_2	123.3(3)			
H6_2	N1_2	C5_2	118.3			
C1_2	C2_2	H2_2	120.6			
C1_2	C2_2	C3_2	118.8(3)			
H2_2	C2_2	C3_2	120.6			
C2_2	C3_2	H3_2	120.2			
C2_2	C3_2	C4_2	119.7(3)			
H3_2	C3_2	C4_2	120.2			
C3_2	C4_2	H4_2	120.3			
C3_2	C4_2	C5_2	119.4(3)			
H4_2	C4_2	C5_2	120.3			
N1_2	C5_2	C4_2	119.2(3)			
N1_2	C5_2	H5_2	120.4			
C4_2	C5_2	H5_2	120.4			

Figure S6. ORTEP drawing of compound **6**, $(C_5H_5NCl)_2[TeBr_6]$.

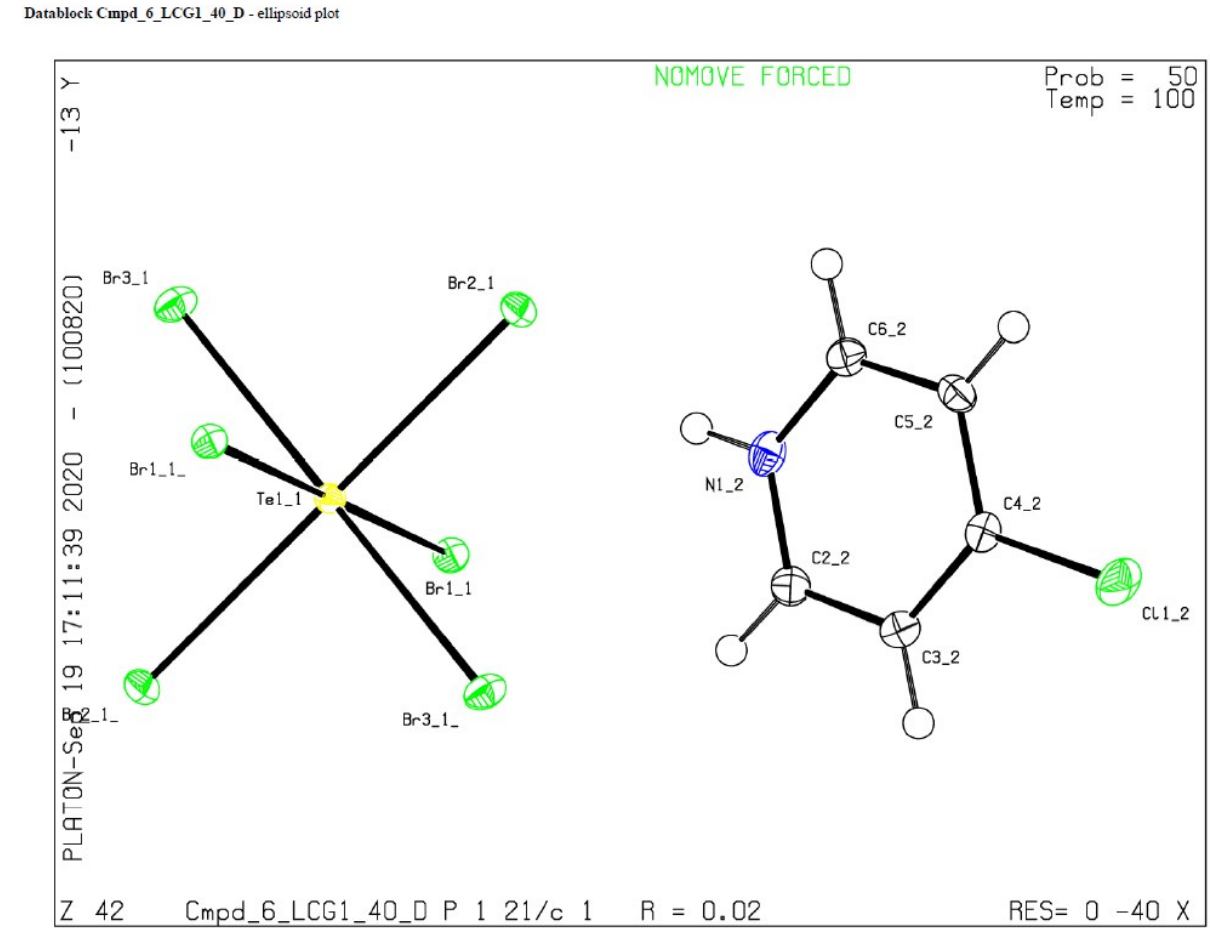

Table S6. Bond distances and angles for compound **6**, $(C_5H_5NCl)_2[TeBr_6]$.

Atom1	Atom2	Atom3	Angle	Atom1	Atom2	Length
Br2_1	Te1_1	Br3_1	89.7	Te1_1	Br2_1	2.6962
Br2_1	Te1_1	Br1_1	92.1	Te1_1	Br3_1	2.691
Br2_1	Te1_1	Br2_1	180.0	Te1_1	Br1_1	2.7157
Br2_1	Te1_1	Br3_1	90.3	Te1_1	Br2_1	2.6962
Br2_1	Te1_1	Br1_1	87.9	Te1_1	Br3_1	2.691
Br3_1	Te1_1	Br1_1	91.6	Te1_1	Br1_1	2.7157
Br3_1	Te1_1	Br2_1	90.3	N1_2	H1_2	0.88
Br3_1	Te1_1	Br3_1	180.0	N1_2	C2_2	1.329(3)
Br3_1	Te1_1	Br1_1	88.4	N1_2	C6_2	1.345(3)
Br1_1	Te1_1	Br2_1	87.9	Cl1_2	C4_2	1.715(2)
Br1_1	Te1_1	Br3_1	88.4	C2_2	H2_2	0.95
Br1_1	Te1_1	Br1_1	180.0	C2_2	C3_2	1.377(3)
Br2_1	Te1_1	Br3_1	89.7	C3_2	H3_2	0.95
Br2_1	Te1_1	Br1_1	92.1	C3_2	C4_2	1.385(3)
Br3_1	Te1_1	Br1_1	91.6	C4_2	C5_2	1.398(3)
H1_2	N1_2	C2_2	118.4	C5_2	H5_2	0.95
H1_2	N1_2	C6_2	118.4	C5_2	C6_2	1.375(3)
C2_2	N1_2	C6_2	123.1(2)	C6_2	H6_2	0.95
N1_2	C2_2	H2_2	119.9			
N1_2	C2_2	C3_2	120.2(2)			
H2_2	C2_2	C3_2	119.9			
C2_2	C3_2	H3_2	120.9			
C2_2	C3_2	C4_2	118.1(2)			
H3_2	C3_2	C4_2	121.0			
Cl1_2	C4_2	C3_2	119.7(2)			
Cl1_2	C4_2	C5_2	119.3(2)			
C3_2	C4_2	C5_2	121.0(2)			
C4_2	C5_2	H5_2	121.0			
C4_2	C5_2	C6_2	118.0(2)			
H5_2	C5_2	C6_2	121.0			
N1_2	C6_2	C5_2	119.6(2)			
N1_2	C6_2	H6_2	120.2			
C5_2	C6_2	H6_2	120.2			

Figure S7. ORTEP drawing of compound **7**, $(C_5H_5NBr)_2[TeBr_6]$.

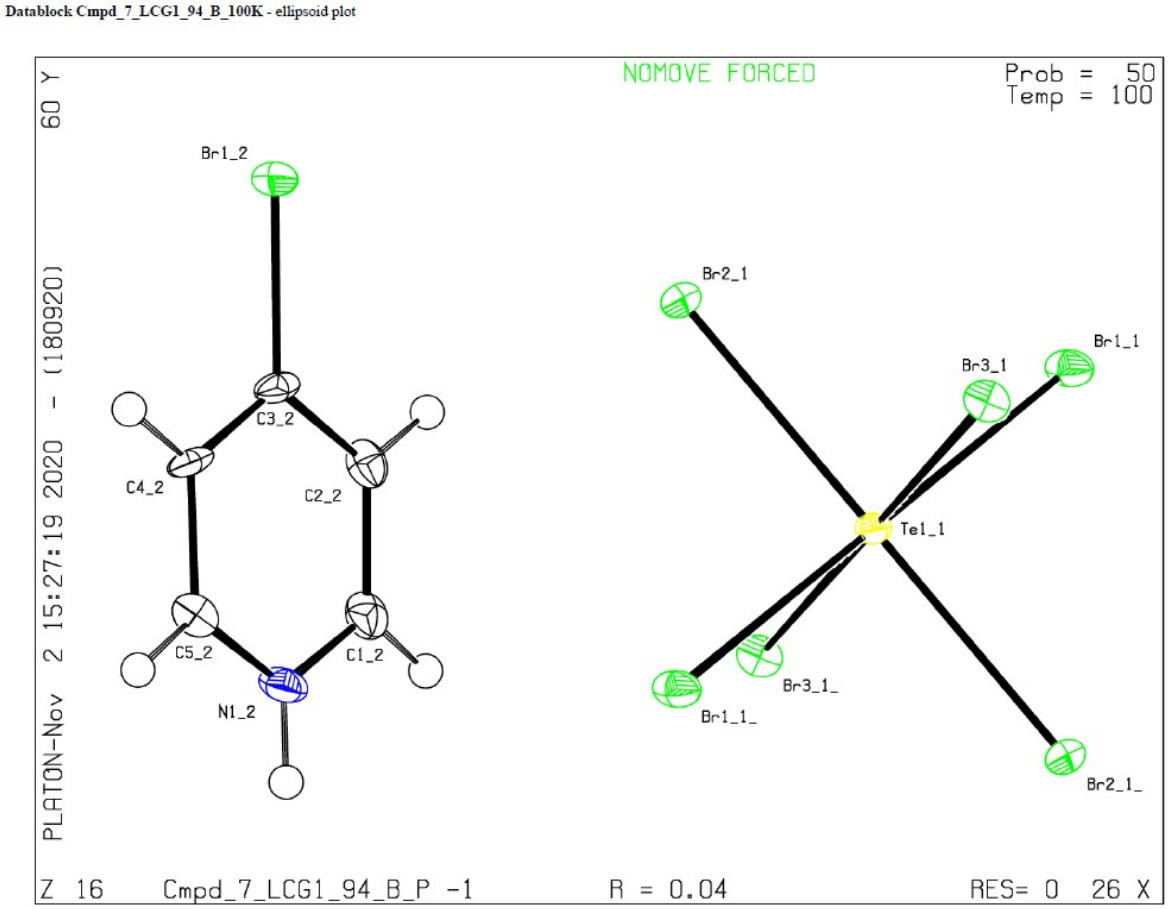

Table S7. Bond distances and angles for compound **7**, $(C_5H_5NBr)_2[TeBr_6]$.

Atom1	Atom2	Atom3	Angle	Atom1	Atom2	Length
Br2_1	Te1_1	Br3_1	87.3	Te1_1	Br2_1	2.6989
Br2_1	Te1_1	Br1_1	89.5	Te1_1	Br3_1	2.711
Br2_1	Te1_1	Br2_1	180.0	Te1_1	Br1_1	2.7006
Br2_1	Te1_1	Br3_1	92.7	Te1_1	Br2_1	2.6989
Br2_1	Te1_1	Br1_1	90.5	Te1_1	Br3_1	2.711
Br3_1	Te1_1	Br1_1	87.7	Te1_1	Br1_1	2.7006
Br3_1	Te1_1	Br2_1	92.7	Br1_2	C3_2	1.885(9)
Br3_1	Te1_1	Br3_1	180.0	C2_2	H2_2	0.95
Br3_1	Te1_1	Br1_1	92.3	C2_2	C3_2	1.38(1)
Br1_1	Te1_1	Br2_1	90.5	C2_2	C1_2	1.37(1)
Br1_1	Te1_1	Br3_1	92.3	C3_2	C4_2	1.39(1)
Br1_1	Te1_1	Br1_1	180.0	C4_2	H4_2	0.95
Br2_1	Te1_1	Br3_1	87.3	C4_2	C5_2	1.38(1)
Br2_1	Te1_1	Br1_1	89.5	C5_2	H5_2	0.95
Br3_1	Te1_1	Br1_1	87.7	C5_2	N1_2	1.35(1)
H2_2	C2_2	C3_2	120.8	C1_2	H1_2	0.95
H2_2	C2_2	C1_2	120.8	C1_2	N1_2	1.330(9)
C3_2	C2_2	C1_2	118.3(8)	N1_2	H6_2	0.88
Br1_2	C3_2	C2_2	119.3(7)			
Br1_2	C3_2	C4_2	119.6(7)			
C2_2	C3_2	C4_2	121.1(8)			
C3_2	C4_2	H4_2	120.7			
C3_2	C4_2	C5_2	118.6(8)			
H4_2	C4_2	C5_2	120.7			
C4_2	C5_2	H5_2	120.9			
C4_2	C5_2	N1_2	118.3(8)			
H5_2	C5_2	N1_2	120.8			
C2_2	C1_2	H1_2	120.2			
C2_2	C1_2	N1_2	119.6(8)			
H1_2	C1_2	N1_2	120.2			
C5_2	N1_2	C1_2	124.1(8)			
C5_2	N1_2	H6_2	118.0			
C1_2	N1_2	H6_2	117.9			

Figure S8. ORTEP drawing of compound **8**, $(C_5H_5NI)_2[TeBr_6]$.

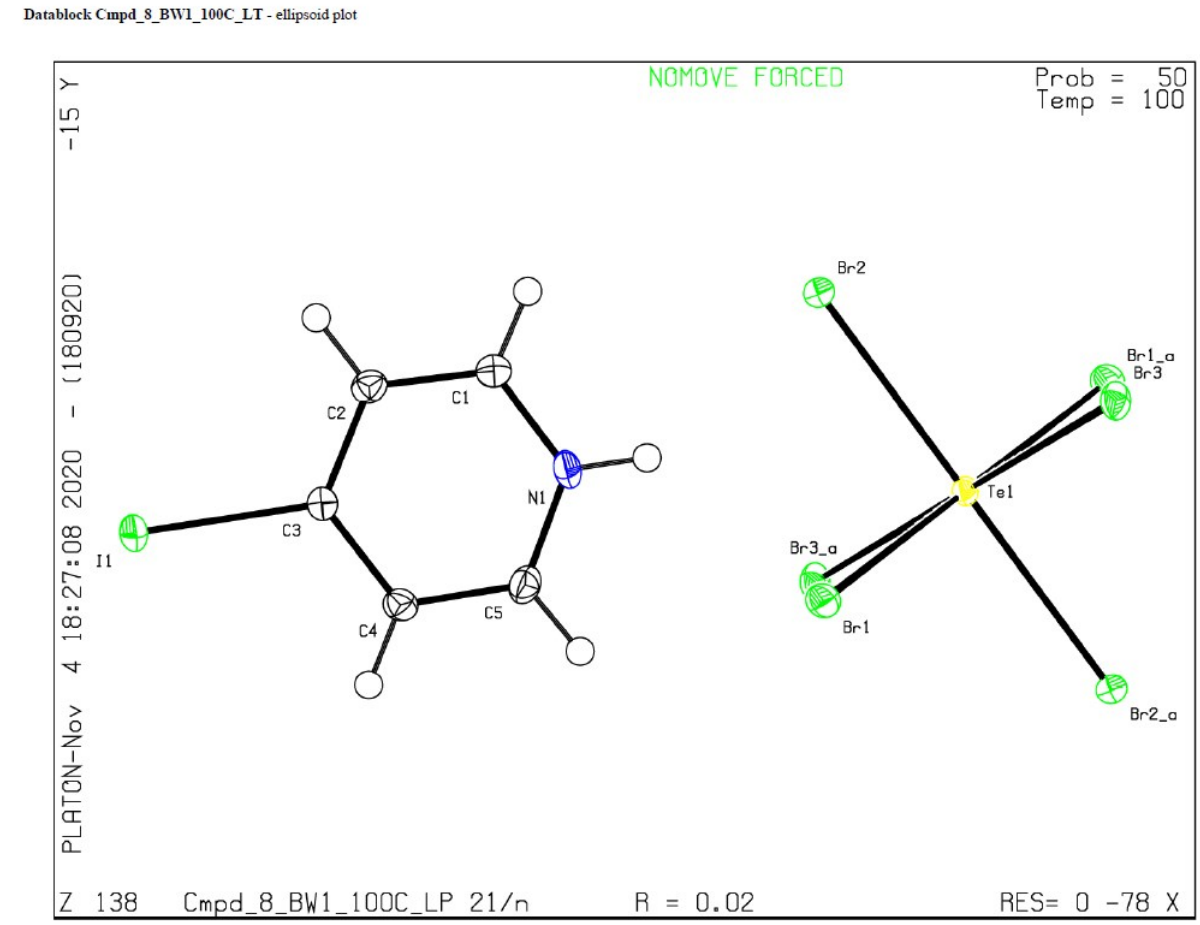

Table S8. Bond distances and angles for compound **8**, $(C_5H_5NI)_2[TeBr_6]$.

Atom1	Atom2	Atom3	Angle	Atom1	Atom2	Length
H6	N1	C1	118.6	I1	C3	2.089(3)
H6	N1	C5	118.6	N1	H6	0.88
C1	N1	C5	122.7(3)	N1	C1	1.344(4)
N1	C1	H1	120.0	N1	C5	1.342(5)
N1	C1	C2	120.0(3)	C1	H1	0.949
H1	C1	C2	120.0	C1	C2	1.371(4)
C1	C2	H2	120.6	C2	H2	0.949
C1	C2	C3	118.8(3)	C2	C3	1.381(5)
H2	C2	C3	120.6	C3	C4	1.397(5)
I1	C3	C2	120.6(2)	C4	H4	0.95
I1	C3	C4	118.9(2)	C4	C5	1.380(5)
C2	C3	C4	120.5(3)	C5	H5	0.949
C3	C4	H4	120.8	Te1	Br1	2.696
C3	C4	C5	118.5(3)	Te1	Br2	2.7082
H4	C4	C5	120.8	Te1	Br3	2.7021
N1	C5	C4	119.5(3)	Te1	Br1	2.696
N1	C5	H5	120.2	Te1	Br2	2.7082
C4	C5	H5	120.2	Te1	Br3	2.7021
Br1	Te1	Br2	87.7			
Br1	Te1	Br3	91.7			
Br1	Te1	Br1	180.0			
Br1	Te1	Br2	92.3			
Br1	Te1	Br3	88.3			
Br2	Te1	Br3	90.5			
Br2	Te1	Br1	92.3			
Br2	Te1	Br2	180.0			
Br2	Te1	Br3	89.5			
Br3	Te1	Br1	88.3			
Br3	Te1	Br2	89.5			
Br3	Te1	Br3	180.0			
Br1	Te1	Br2	87.7			
Br1	Te1	Br3	91.7			
Br2	Te1	Br3	90.5			

Table S9. Hydrogen bonding parameters for compounds **1**-**8**.

Compound	Donor Atom	Atom 2	D-A Dist. (Å)	Angle (°)	Compound	Donor Atom	Atom 2	D-A Dist. (Å)	Angle (°)
1	N1 (H1)	Cl2	3.380(5)	123.0	**5**	N1 (H1)	Br1	3.498(2)	127.1
	N1 (H1)	Cl1	3.406(4)	137.4		N1 (H1)	Br1 (2)	3.620(2)	136.0
	N1 (H1)	Cl1 (2)	3.252(6)	117.8		N1 (H1)	Br3	3.381(3)	117.8
	C1 (H1)	Cl2 (2)	3.412(7)	121.4		C6 (H6)	Br2	3.638(2)	133.4
	C3 (H2)	Cl2 (3)	3.759(6)	150.2		C5 (H5)	Br3 (2)	3.803(2)	151.0
	C4 (H4)	Cl2 (4)	3.673(6)	150.2		C2(H2)	Br3 (3)	3.499(3)	121.4
	C5 (H5)	Cl3	3.512(5)	132.1					
2	N1 (H6)	Cl2	3.248(1)	138.7	**6**	N1 (H1)	Br1	3.405(2)	139.3
	N1 (H6)	Cl2 (2)	3.314(1)	132.4		N1 (H1)	Br1 (2)	3.460(2)	133.2
	C2 (H2)	Cl3	3.438(2)	124.8		C2 (H2)	Br1 (3)	3.596(3)	118.1
	C5 (H5)	Cl3 (2)	3.601(2)	149.3		C2 (H2)	Br3	3.566(3)	124.9
						C3 (H3)	Br1 (4)	3.923(2)	156.3
						C5 (H5)	Br3 (2)	3.740(2)	145.8
3	N1 (H1)	Cl2	3.235(3)	137.8	**7**	N1 (H6)	Br3	3.456(7)	144.0
	N1 (H1)	Cl2(1)	3.259(3)	134.2		N1 (h6)	Br1	3.481(8)	130.4
	C2 (H2)	Cl1	3.559(3)	128.0		C1 (H1)	Br1 (2)	3.550(8)	121.0
	C4 (H4)	Cl3 (2)	3.728(3)	160.4		C1 (H1)	Br3 (2)	3.681(8)	126.5
	C5 (H5)	Cl1 (2)	3.653(3)	149.2		C2 (H2)	Br3' (3)	3.813(7)	172.4
						C4 (H4)	Br1 (2)	3.737(8)	154.7
4	N1 (H1A)	Cl1	3.214(3)	147.7	**8**	N1 (H6)	Br3	3.551(3)	120.7
	N1 (H1A)	Cl3	3.473(3)	125.1		N1 (H6)	Br2	3.369(3)	144.5
	C2 (H2)	Cl1 (2)	3.531(3)	133.3		C1 (H1)	Br1	3.660(3)	135.7
	C4 (H4)	Cl2 (2)	3.629(3)	138.0		C2 (H2)	Br3 (2)	3.700(3)	141.1
	C5 (H5)	Cl3 (2)	3.553(3)	130.1		C4 (H4)	Br2 (2)	3.675(4)	130.6

Table S10. Halogen···π bonding parameters for relevant compounds.

Compound	Atom 1	Atom 2	Dist. (Å)	Te-X-Ring Atom Angle (°)
2	Cl1	N1	3.289(2)	96.37
	Cl1	C6	3.410(2)	119.23
3	Cl3	C1	3.408(4)	117.23
6	Br2	N1	3.391(3)	94.88
	C5 (H5)	C5	3.527(3)	117.07
7	Br1	C5	3.44(1)	102.6

Figure S9. Electrostatic potential of $[TeX_6]^{2-}$ in **1-8** mapped onto a 0.002 ε $bohr^{-1}$ isodensity surface. Octahedral orientation shown at left. Cl = green, Br = brown, and Te = orange. Regions of rich electron density are highlighted as areas of red while electron deficient areas are blue.

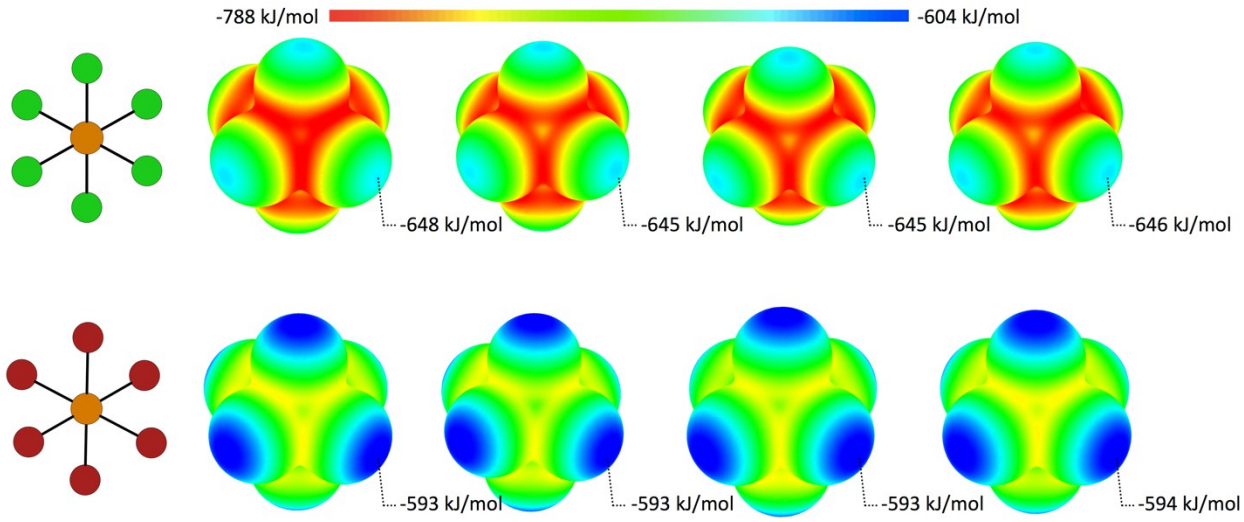

Figure S10. Tauc plot of **1-9** derived from the solid-state DRS data showing the optical absorption edge.

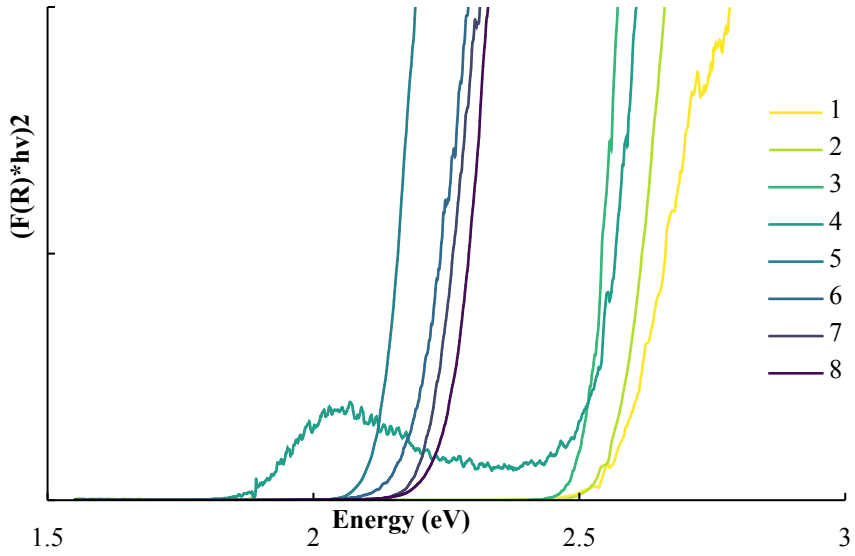

Figure S11. Cationic molecular models of **1-8** containing an isolated $[TeX_6]^{2-}$ octahedra surrounded by noncovalent interacting pyridinium used for NBO, NLMO, SOPT, and QTAIM calculations.

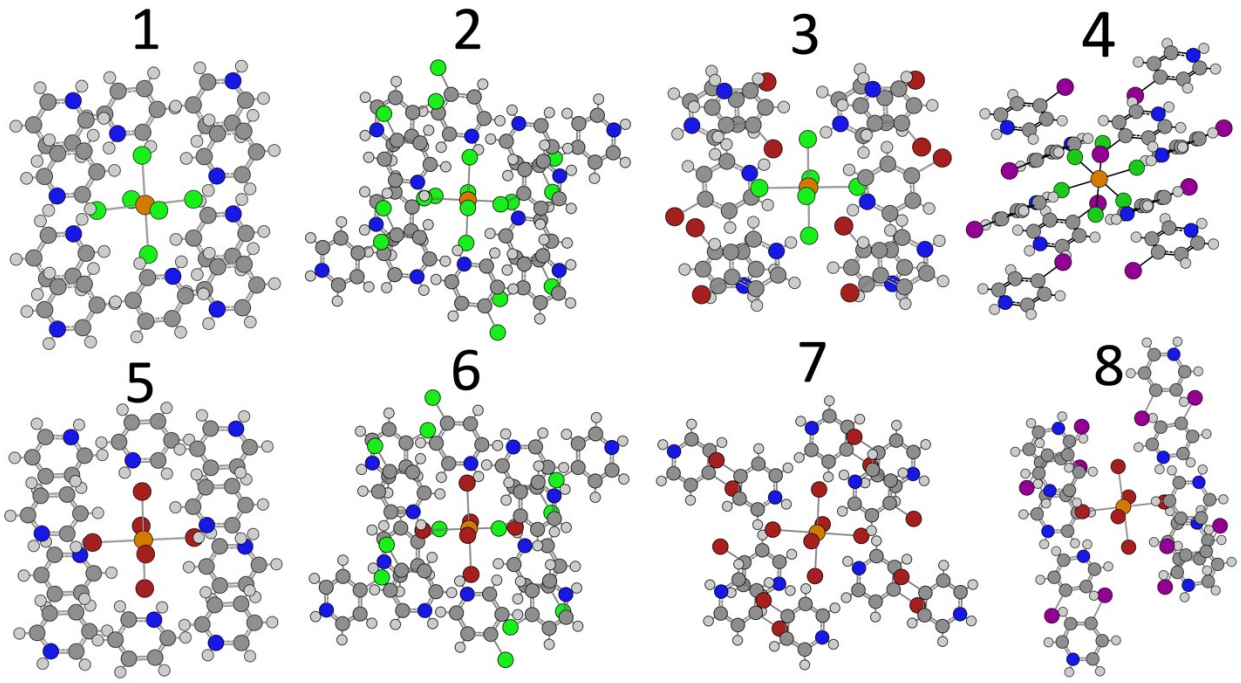

Table S11. QTAIM metrics for the three crystallographically unique Te-X bonds in **1-8**.

Compound	Metal-Halide	Cation	WBI	e^- Density	Laplacian
1	TeCl	HPY	0.5118	0.07154265	0.06986931
1	TeCl	HPY	0.5117	0.06766289	0.06432752
1	TeCl	HPY	0.5103	0.07072789	0.06894772
2	TeCl	ClPY	0.4908	0.07038019	0.06793610
2	TeCl	ClPY	0.5165	0.06658695	0.06517231
2	TeCl	ClPY	0.5205	0.07100542	0.06819041
3	TeCl	BrPY	0.4899	0.07041394	0.06770214
3	TeCl	BrPY	0.5164	0.06697729	0.06548365
3	TeCl	BrPY	0.5199	0.07026630	0.06783113
4	TeCl	IPY	0.5097	0.06988452	0.06645121
4	TeCl	IPY	0.529	0.06897080	0.06646125
4	TeCl	IPY	0.4885	0.06906160	0.06851784
5	TeBr	HPY	0.5355	0.06186135	0.05014013
5	TeBr	HPY	0.5312	0.05923954	0.04702737
5	TeBr	HPY	0.5307	0.06286828	0.05069984
6	TeBr	ClPY	0.5158	0.06133124	0.04947931
6	TeBr	ClPY	0.5349	0.06167234	0.04928240
6	TeBr	ClPY	0.5389	0.05894412	0.04825775
7	TeBr	BrPY	0.5408	0.06060681	0.04937088
7	TeBr	BrPY	0.5165	0.06048530	0.04821159
7	TeBr	BrPY	0.5293	0.06145642	0.04939613
8	TeBr	IPY	0.5105	0.06185702	0.04896172
8	TeBr	IPY	0.5213	0.06018530	0.04934469
8	TeBr	IPY	0.5491	0.06108287	0.04952431

Table S12. NLMO metrics of **1-8**.

			Halide			Metal	
	Cation	Te-X	% Contribution	*% s*-orbital	*% p*-orbital	% Contribution	*%p*-orbital
1	Py	Te1-Cl2	80.022	11.72	88.03	18.731	98.00
1	Py	Te1-Cl6	80.828	13.59	86.18	18.037	97.92
1	Py	Te1-Cl4	80.653	13.39	86.41	18.125	97.93
2	ClPY	Te1-Cl2	79.908	12.31	87.48	17.989	98.09
2	ClPy	Te1-Cl6	79.331	12.94	86.82	18.440	97.91
2	ClPy	Te1-Cl4	78.559	12.93	86.85	18.295	97.94
3	BrPy	Te1-Cl3	80.052	12.28	87.49	17.947	98.05
3	BrPy	Te1-Cl5	79.279	12.85	86.92	18.444	97.93
3	BrPy	Te1-Cl4	79.466	13.04	86.74	18.570	98.00
4	IPy	Te1-Cl6	79.640	12.36	87.41	18.368	97.96
4	IPy	Te1-Cl7	81.032	12.45	87.36	17.626	98.01
4	IPy	Te1-Cl2	79.097	12.16	87.58	18.894	97.91
5	Py	Te1-Br5	75.824	9.23	90.50	22.349	98.10
5	Py	Te1-Br6	77.139	11.23	88.57	21.223	98.06
5	Py	Te1-Br4	76.852	11.00	88.83	21.423	98.10
6	ClPy	Te1-Br2	75.320	10.00	89.78	21.714	98.23
6	ClPy	Te1-Br6	75.155	10.43	89.36	21.795	98.06
6	ClPy	Te1-Br4	73.551	10.45	89.35	22.959	98.29
7	BrPy	Te1-Br5	76.007	9.69	90.05	22.249	98.08
7	BrPy	Te1-Br4	76.521	10.13	89.67	21.653	98.09
7	BrPy	Te1-Br3	77.187	10.71	89.10	21.202	98.14
8	IPy	Te4-Br5	77.408	10.73	89.08	21.000	98.15
8	IPy	Te4-Br6	77.472	9.96	89.80	16.342	96.66
8	IPy	Te4-Br3	78.091	9.89	89.95	15.924	96.91

Table S13. Second Order Perturbation Theory derived stabilization energies of noncovalent interactions for compounds **1-8**. Data are reported for the total stabilization energy (X-bonding + H-bonding) as well as the individual contributing interactions by type (X-bonding or H-bonding). Values were extracted for the three crystallographically unique Te-X bonds.

				Stabilization Energy (kCal/mol)				
Compound	**Metal-Halide**	**Cation**	**Atom**	**X-X**	**X-H**	**X-C**	**X-π**	**Total**
1	TeCl	HPY	Cl1	0.00	1.73	0.56	0.30	2.59
1	TeCl	HPY	Cl2	0.00	1.06	0.74	0.36	2.16
1	TeCl	HPY	Cl3	0.00	1.88	0.13	1.21	3.22
2	TeCl	ClPY	Cl1	0.47	3.86	0.64	0.00	4.97
2	TeCl	ClPY	Cl2	0.35	0.87	0.36	0.98	2.56
2	TeCl	ClPY	Cl3	0.00	1.78	0.30	1.08	3.16
3	TeCl	BrPY	Cl1	3.13	3.61	0.71	0.05	7.50
3	TeCl	BrPY	Cl2	0.00	1.68	0.72	0.25	2.65
3	TeCl	BrPY	Cl3	0.14	1.76	0.36	0.31	2.57
4	TeCl	IPY	Cl1	0.00	1.39	0.69	0.22	2.30
4	TeCl	IPY	Cl2	0.00	3.21	0.40	0.33	3.94
4	TeCl	IPY	Cl3	2.54	1.23	0.41	0.40	4.58
5	TeBr	HPY	Br1	0.00	1.76	0.64	0.09	2.49
5	TeBr	HPY	Br2	0.00	2.08	0.17	1.41	3.66
5	TeBr	HPY	Br3	0.00	1.55	0.78	0.53	2.86
6	TeBr	ClPY	Br1	0.56	4.32	0.72	0.00	5.60
6	TeBr	ClPY	Br2	0.00	1.76	0.31	1.37	3.44
6	TeBr	ClPY	Br3	0.48	1.03	0.35	1.10	2.96
7	TeBr	BrPY	Br1	0.00	3.86	0.25	0.58	4.69
7	TeBr	BrPY	Br2	0.00	2.59	0.51	1.05	4.15
7	TeBr	BrPY	Br3	2.05	0.64	0.25	0.98	3.92
8	TeBr	IPY	Br1	0.00	5.97	0.34	0.83	7.14
8	TeBr	IPY	Br2	2.30	1.41	0.26	0.44	4.41
8	TeBr	IPY	Br3	0.00	1.54	0.37	0.35	2.26

Time-Dependent Density Functional Theory (TD-DFT) Details.

The molecular transitions of metal halide anions in **1** and **5**, as the only complexes featuring X···X interactions between $[TeX_6]^{2-}$ units, were calculated using TD-DFT within the Gaussian16 software. The def2-TZVP basis set was utilized with the B3LYP functional as described in the computational methods. Structure optimization was performed on four models constructed using the XRD data of **1** and **5** prior to time-dependent calculations as shown in Figure S12. These models were constructed of either an isolated $[TeX_6]^{2-}$ monomer or a dimeric unit consisting of two adjacent $[TeX_6]^{2-}$ octahedra featuring an X···X interaction. Optimization calculations of the highly anionic dimeric models utilized frozen Te coordinates to overcome electrostatic repulsion.

Calculated UV-vis spectra (Figure S13) feature two dominant band bands in both monomeric and dimeric models. For the TeCl species these bands occur at approximately 190 nm and 310 nm, while for those for the TeBr species occur at 230 nm and 360 nm. TD-DFT calculated molecular orbital transitions (Figure S13-S14) reveal that the high energy band can be generally assigned as a halide to metal/halide charge transfer where the donor orbitals reside largely on the halides as lone pair n*p* orbitals, and the acceptor orbitals are a combination of Te^{4+} *p* and halide (n+1)*p* orbitals. The less intense lower energy band can be described as a hybridized cluster centered transition typical of close related bismuth(III) halide clusters[1,2] involving the electronic rearrangement of metal and halide valance orbitals. Here, the donor orbitals are clearly Te^{4+} *s* and halide *p* in character and agree with the DOS calculations of the hybrid materials. The acceptor orbitals for the lower energy band contains significant metal *p*-character. Notably, the dimeric TeBr acceptor contains a Te-Br σ^* orbital that *bridges* $[TeBr_6]^{2-}$ units, indicating possible electron delocalization across the X···X interactions in the absence of pyridinium π^* acceptor orbitals.

Figure S12. B3LYP/def2-TZVP optimized $[TeX_6]^{2-}$ monomer and $[TeX_6\cdots TeX_6]^{4-}$ dimer models used for TD-DFT calculated UV-vis spectra.

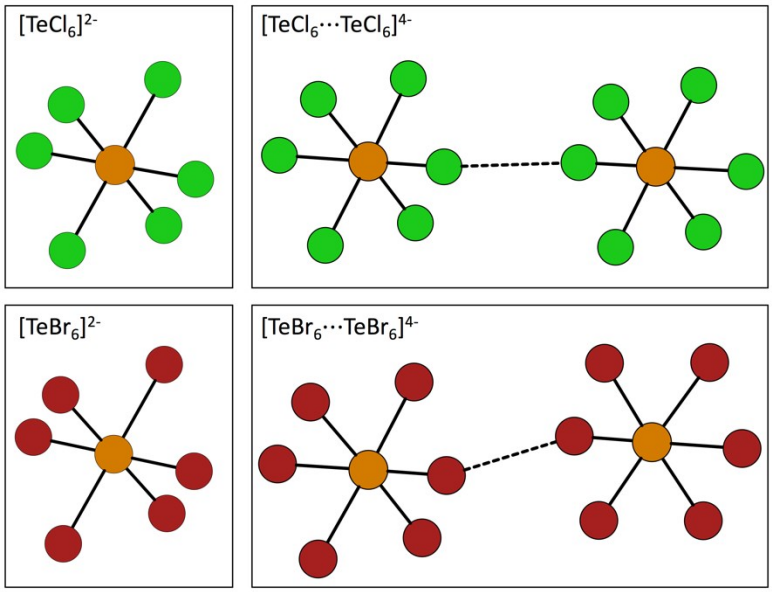

Figure S13. TD-DFT B3LYP/def2-TZVP calculated UV-vis spectra of $[TeX_6]^{2-}$ monomer and $[TeX_6\cdots TeX_6]^{4-}$ dimer models.

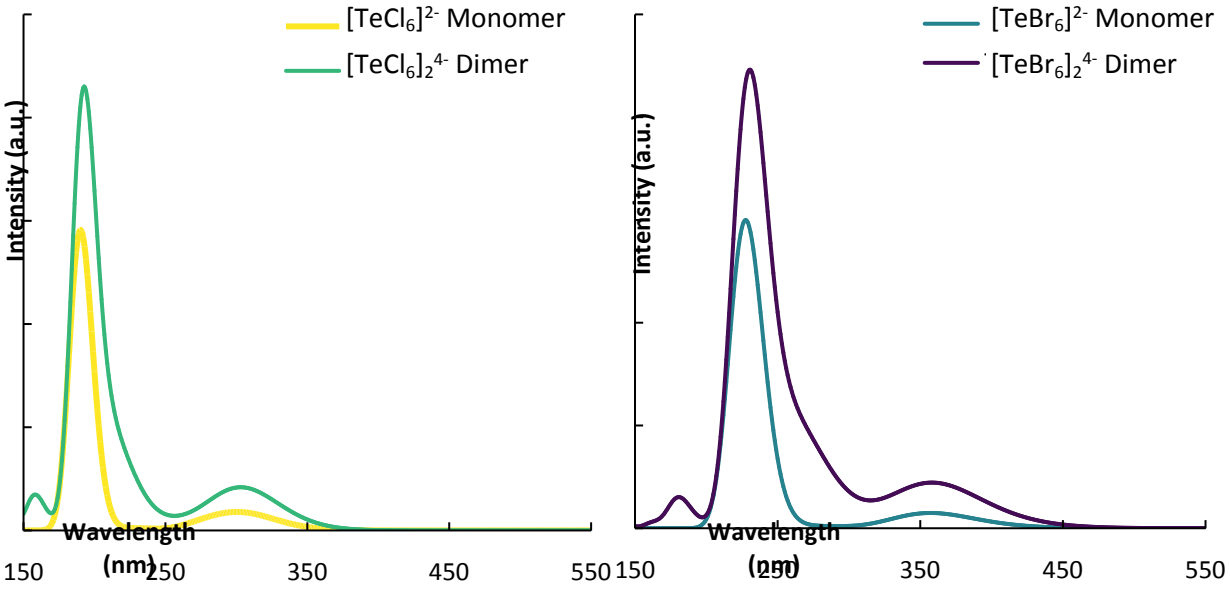

Table S14. TD-DFT B3LYP/DEF2-TZVP transitions for calculated excited states (oscillation > 0.1) corresponding to dominant UV-vis band energies.

Model	Excited State	Energy	Donor		Acceptor	Coefficient	Contribution*	Oscillation
$[TeCl_6]^{2-}$	1	308 nm	53	→	67	0.15769	5%	0.587
			61	→	66	-0.15636	5%	
			62	→	65	-0.15636	5%	
			64	→	67	0.65059	85%	
	43	190 nm	50	→	66	0.14090	4%	1.1974
			51	→	65	0.14090	4%	
			53	→	67	0.58896	74%	
			54	→	67	0.20263	9%	
			64	→	67	-0.20759	9%	
$[TeCl_6\cdots TeCl_6]^{4-}$	3	318 nm	127	→	129	-0.14824	5%	0.0910
			127	→	130	-0.25889	15%	
			127	→	131	-0.23388	13%	
			128	→	129	0.52389	63%	
			128	→	133	-0.13110	4%	
	169	200 nm	100	→	129	0.17438	7%	0.3850
			100	→	133	0.24523	14%	
			101	→	134	0.40789	38%	
			107	→	134	0.42747	42%	
$[TeBr_6]^{2-}$	10	356 nm	108	→	120	-0.23392	11%	0.0562
			115	→	121	-0.30794	19%	
			117	→	119	-0.30794	19%	
			118	→	120	0.49362	50%	
	43	228 nm	104	→	121	-0.12345	3%	1.2340
			106	→	119	-0.12345	3%	
			107	→	120	0.22585	11%	
			108	→	120	0.58140	71%	
			118	→	120	0.24408	12%	
$[TeBr_6\cdots TeBr_6]^{4-}$	10	386 nm	230	→	238	0.10541	3%	0.0347
			230	→	240	0.10673	3%	
			231	→	242	-0.10263	2%	
			233	→	237	-0.10389	2%	
			233	→	241	-0.19067	8%	
			235	→	239	-0.32326	24%	
			236	→	237	0.46532	50%	
			236	→	241	-0.18867	8%	
	44	335 nm	223	→	240	-0.10852	3%	0.0268
			224	→	239	0.31805	24%	
			225	→	237	0.29736	21%	
			227	→	238	-0.17971	8%	
			232	→	240	-0.29808	21%	
			234	→	238	0.27999	18%	
			234	→	240	-0.12028	3%	
			236	→	241	0.10226	2%	

*Percent contribution is calculated by the square of the coefficient divided by the sum of squared coefficients.

Figure S14. TD-DFT B3LYP/DEF2-TZVP molecular orbital isodensity representations of dominant transitions for $[TeCl_6]^{2-}$ (top) and $[TeCl_6\cdots TeCl_6]^{4-}$ (bottom) calculated excited states. Energy and contribution of transition noted.

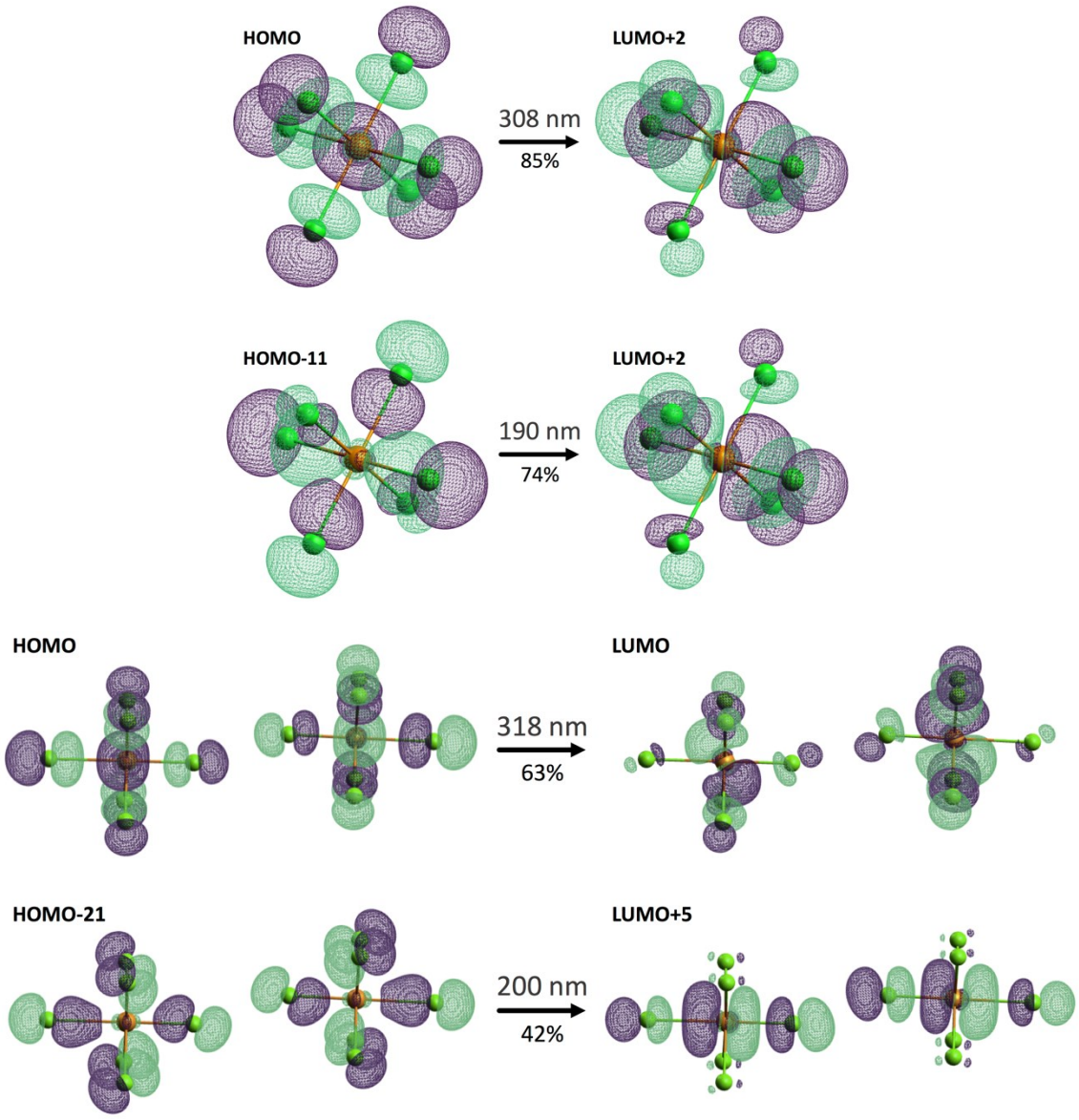

Figure S15. TD-DFT B3LYP/DEF2-TZVP molecular orbital isodensity representations of dominant transitions for $[TeBr_6]^{2-}$ (top) and $[TeBr_6\cdots TeBr_6]^{4-}$ (bottom) calculated excited states.

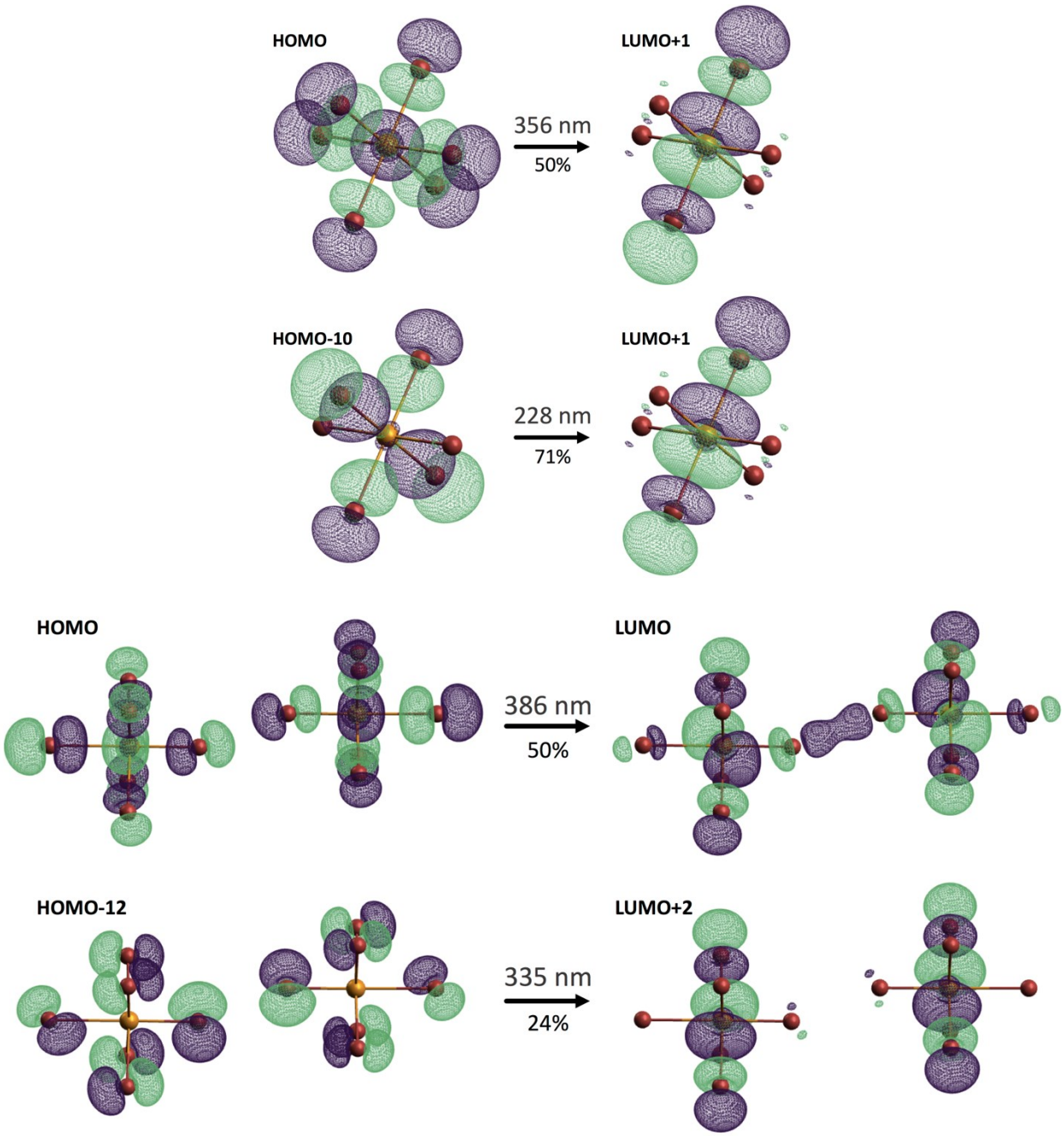

Quantum Theory of Atoms in Molecules (QTAIM) Details.

QTAIM calculations were performed using NBO7 and Multiwfn software on building units of **1-8** constructed from crystallographic fragments (Figure S11). The QTAIM metrics for the crystallographically unique Te-X bonds address the relative bond strengths across the series and highlight a number of trends in relation to TeX composition and noncovalent interaction strength. A comparison of the Wiberg bond index, electron density, $\rho(r)$, and Laplacian of the density, $\nabla^2\rho$, at the bond critical points (BCP) provided by QTAIM for **1-8** are shown in Table S15. Initially developed for closed-shell semi-empirical wavefunctions, the Wiberg bond index is a convenient topological analysis metric for determining bond strengths,[3] and is a function of electron population overlap between atom pairs where greater overlap yields subsequent higher index values, and is closely related to formal bond order. Despite compounds **1-8** featuring similar metal - halide coordination, variations in Wiberg Bond indexes are indeed observed across the series. Of the $[TeX_6]^{2-}$ species, the bromo ligands feature the greatest bond indexes and lowest $\rho(r)$ values in comparison to the chloro analogs, initially indicating a *stronger* metal-halide bond. The topological analysis reveals that the Wiberg and $\rho(r)$ values decrease for both $[TeX_6]^{2-}$ species as the pyridinium substituent becomes more polarizable on the order of H > Cl > Br > I, implying that second sphere coordination via NCIs are able to influence inner sphere Te-X bonding. Of particular note, the larger index values for the $[TeBr_6]^{2-}$ species occur, per contra, with a marked reduction in electron density when compared to the $[TeCl_6]^{2-}$ species. At first glance this divergent behavior is counter intuitive to our understanding of bond order and electron density where higher ordered bonds arise *because of* increased electron density. The Wiberg bond index (*W*) is a product of the summation over the atomic orbitals μ and ν on atom A and atom B, respectively, and the square of the corresponding density matrix element (*P*) (Equation 1).

$$W = \sum_{\mu \in A} \sum_{\nu \in A} P_{\mu\nu}^{2} \qquad (1)$$

Inspection of the Wiberg expression reveals that an increase in index value accompanied by a reduction in total electron density can only occur if the orbital overlap is increased sufficiently to offset the loss of density between the atom pairs. Furthermore, to maintain a lower electron density, the increased overlap would need to involve atomic orbitals on either or both atoms having a lower electron density at the BCP.

Table S15. Averaged QTAIM metrics at the bond critical points for **1-8**.

	Atom Pair	Wiberg	$\rho(r)$	$\nabla^2\rho$
1	Te···Cl	0.5113	0.0700	0.0677
2	Te···Cl	0.5093	0.0693	0.0671
3	Te···Cl	0.5087	0.0692	0.0670
4	Te···Cl	0.5068	0.0683	0.0662
5	Te···Br	0.5325	0.0613	0.0493
6	Te···Br	0.5299	0.0606	0.0490
7	Te···Br	0.5289	0.0608	0.0490
8	Te···Br	0.5270	0.0610	0.0493

To reconcile the conflicting Wiberg and electron densities, two possible mechanisms may be considered: (i) a change in atomic orbital hybridization on *either* atom or (ii) a shift in contribution of empty Te^{4+} 5*p* orbitals to metal-halide coordination. Considering hybridization first, as has been described elsewhere[4], the radial density distribution of hybridized atomic orbitals increases the further away from the central atom on the order $sp < sp^2 < sp^3$. Thus, greater atomic hybridization may reduce electron density while simultaneously increasing orbital overlap. Since the coordination geometry about Te^{4+} is symmetrical in **1-8**, the metal *s* lone pairs must remain spherically distributed about the metal center across the series, and are thus unhybridized.[5,6] As such, any loss of electron density owing to hybridization would have to originate at the *halide*. It is equally possible that the loss of electron density is due to the greater contribution of an empty Te^{4+} *p* orbital to form the molecular bond. Here increased *p*-character from the metal center (which contains no electrons), would effectively *lower* the overall electron density while potentially increasing the Wiberg bond index. NLMO calculations demonstrate that both a change in halide atomic orbital hybridization and a shift in empty Te^{4+} 5*p* orbital contribution occur across the series.

DFT Derived Noncovalent Interaction Strength Details.

In addition to the NBO methodology described herein, we also calculated hydrogen and halogen bonding strength using previously reported DFT methods[7] as an effort to bridge past and future efforts to quantify these interactions. The def2-TZVP basis set was utilized with the B3LYP functional as described in the computational methods using Gaussian16. Crystal structures were truncated into geometric clusters to calculate interaction strength and are shown in Figure S16. Interaction strengths are tabulated in Table S16. These interactions are a sum of noncovalent interaction strength *as well as* electrostatic (Coulombic) attraction and thus, should be interpreted with care.

Figure S16. Molecular clusters used to calculate hydrogen and halogen bond energies of **1-8** via DFT.

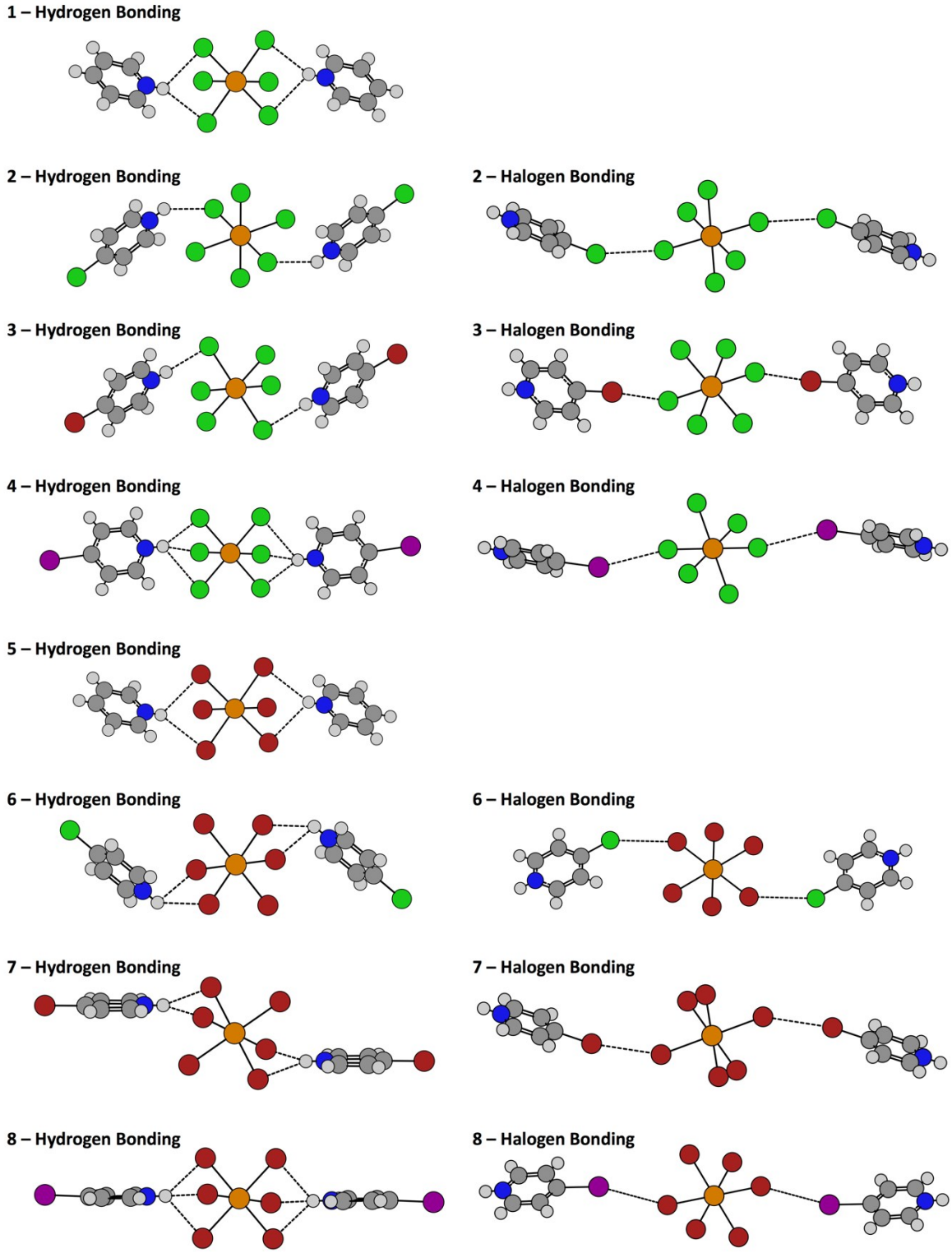

Table S16. DFT calculated hydrogen and halogen bond energies.

Complex	Hydrogen Bonding	Halogen Bonding
1	230 kJ/mol	-
2	211 kJ/mol	70 kJ/mol
3	238 kJ/mol	103 kJ/mol
4	241 kJ/mol	87 kJ/mol
5	216 kJ/mol	-
6	227 kJ/mol	72 kJ/mol
7	227 kJ/mol	76 kJ/mol
8	229 kJ/mol	85 kJ/mol

References

1 A. W. Kelly, A. M. Wheaton, A. D. Nicholas, H. H. Patterson and R. D. Pike, *J. Inorg. Organomet. Polym. Mater.*, 2018, **28**, 528–534.

2 A. W. Kelly, A. M. Wheaton, A. D. Nicholas, F. H. Barnes, H. H. H. Patterson and R. D. Pike, *Eur. J. Inorg. Chem.*, 2017, **2017**, 4990–5000.

3 K. B. Wiberg, *Tetrahedron*, 1968, **24**, 1083–1096.

4 W. E. Palke, *Croat. Chem. Acta*, 1984, **5**, 779–786.

5 L. Shimoni-Livny, J. P. Glusker and C. W. Bock, *Inorg. Chem.*, 1998, **37**, 1853–1867.

6 R. L. Davidovich, V. Stavila, D. V. Marinin, E. I. Voit and K. H. Whitmire, *Coord. Chem. Rev.*, 2009, **253**, 1316–1352.

7 R. G. Surbella, L. C. Ducati, K. L. Pellegrini, B. K. McNamara, J. Autschbach, J. M. Schwantes and C. L. Cahill, *J. Am. Chem. Soc.*, 2017, **139**, 10843–10855.